Review of
Scientific Instruments

ARTICLE

pubs.aip.org/aip/rsi

A new experiment to enable rapid systematic investigations of flux trapping dynamics for superconducting radio-frequency cavity applications

Cite as: Rev. Sci. Instrum. 95, 093902 (2024); doi: 10.1063/5.0202546
Submitted: 5 February 2024 • Accepted: 22 August 2024 •
Published Online: 10 September 2024

F. Kramer,[1,a)] S. Keckert,[1] O. Kugeler,[1] and J. Knobloch[1,2]

AFFILIATIONS

[1] Helmholtz-Zentrum Berlin für Materialien und Energie GmbH, Hahn-Meitner-Platz 1, 14109 Berlin, Germany
[2] Universität Siegen, Department Physik, Walter-Flex-Str. 3, 57068 Siegen, Germany

[a)] **Author to whom correspondence should be addressed:** f.kramer@helmholtz-berlin.de

ABSTRACT

Many modern accelerators rely on superconducting radio-frequency (SRF) cavities to accelerate particles. When these cavities are cooled to the superconducting state, a fraction of the ambient magnetic field (e.g., Earth's magnetic field) may be trapped in the superconductor. This trapped flux can significantly increase the power dissipation of the SRF cavities. It is, therefore, crucial to understand the underlying mechanism of how magnetic flux is trapped and what treatments and operating conditions can reduce the flux-trapping efficiency. A new experiment was designed that enables a systemic investigation of flux trapping. It allows for independent control of cooldown conditions, which might have an influence on flux trapping: temperature gradient across the superconductor during cooldown, cooldown rate, and ambient magnetic field. For exhaustive studies, the setup was designed for quick thermal cycling, permitting up to 300 superconducting transitions in one day. In this paper, the setup and operation is described in detail and an estimation of the measurement errors is given. Exemplary data are presented to illustrate the efficacy of the system.

I. INTRODUCTION

Ideally, a superconducting radio-frequency (SRF) cavity cooled down in any external magnetic field will fully expel all magnetic flux when it transitions from the normal-conducting to the superconducting state. However, the material used for fabrication of the cavities always contains defects or contaminants, which act as pinning centers. At these pinning centers, quantized magnetic flux lines can be stopped if the pinning force compensates the force pushing the flux out of the superconductor. These flux lines are not expelled during cooldown.[1] During cavity operation, the radio frequency (RF) field then forces these trapped flux lines to oscillate, which dissipates power that must be cooled by the helium bath.[2]

In modern SRF cavities, trapped flux frequently is a significant contributor to the total dissipated power in the cavity walls, even in magnetically shielded cryomodules.[3] Given the unavoidable inefficiency of cryoplants, it is crucial to understand the mechanism of flux trapping so that methods can be identified that decrease and ideally altogether eliminate trapped flux in SRF cavities. This can include improvements in the material, and its treatment, as well as modifying the cooldown conditions to force flux expulsion.

Such studies require many SC-NC cycles to explore the wide parameter space known to impact the trapping efficiency. Experiments with cavities[4,5] are cumbersome, expensive, slow, and the data interpretation is complicated due to their complex geometry.[6] Thus, they are ill-suited for studies designed to understand the fundamentals of flux trapping in superconductors. We, therefore, decided to design an apparatus for flat samples to allow for a far more extensive and systematic investigation.[7] This system provides several advantages. 1. The samples are smaller, so less material is needed but they are large enough to study macroscopic effects. 2. Since the samples are flat sheets, treatments are easier to apply compared to cavities. In addition, the impact of geometry can be isolated easier. 3. Cooldown parameters are easier to control. 4. The thermal cycles can be performed much quicker, allowing for ≈300 cooldowns per day instead of only ≈5 per day with cavities. The results gained with this apparatus should improve the understanding of flux trapping in general, as well as trapped flux in SRF cavities. However, for the latter, the measurements need to be complemented by tests with cavities to address the specifics of their geometry and production steps. The combination of these results should help evaluate whether it is possible to operate an SRF cavity with reduced magnetic shielding.

The disadvantage is that no RF surface resistance can be measured with this setup, i.e., we cannot determine the impact of flux trapping on the power dissipation. For example, a cavity manufactured from a material that expels flux well but has a high sensitivity of surface resistance to trapped flux might dissipate more power due to trapped flux than a cavity manufactured from a material with worse flux expulsion properties but lower sensitivity of surface resistance to trapped flux.

The setup is designed to measure trapped flux as a function of five parameters: temperature gradient during cooldown, cooldown rate, external magnetic field, material, and material treatment, where the external magnetic field can be varied both in magnitude an orientation. The first three parameters have to be controlled by the setup directly during measurement. The last two are given by the sample.

While the scientific results obtained with this apparatus have been discussed in detail in Ref. 8, the aim of this paper was to provide a more in-depth description of the actual system and its characterization. At the end of this paper, we briefly review some exemplary measurement results to illustrate the system's capabilities, without claiming completeness.

II. EXPERIMENTAL INFRASTRUCTURE

Before the experimental setup itself is described, the experimental infrastructure is introduced. This includes everything not part of the core setup, which may be used for other experiments.

A. Cryostat

As state-of-the-art cavities are manufactured from niobium, the initial investigation concentrated on this. Since niobium has a critical temperature T_c of 9.2 K, helium must be used to cool the sample. In this case, it is achieved by suspending the sample above a liquid helium bath so that the sample is only cooled by the cold helium gas evaporating from the bath. A glass cryostat with a liquid nitrogen cooled jacket and an aluminum housing provides the required thermal insulation (Fig. 1).

B. Active field compensation

Since the cryostat has no magnetic shielding, the ambient magnetic field must be compensated actively with current-carrying coils.

For the two coils that generate the field in the horizontal plane, a rectangular Helmholtz-coil (HHC) design is chosen. This design achieves high field flatness at the sample position (see in the following) and can be better integrated in the infrastructure of the cryostat than a round Helmholtz-coil design. For the coil that applies a field in the vertical direction, a solenoid design is chosen. Due to the fact that it is realized by winding an insulated copper wire around the aluminum shielding of the cryostat, it occupies nearly no space around the cryostat while still achieving high field flatness. Figure 1 shows a picture of the three coils. The design parameters of the different coils are discussed in more detail in the following.

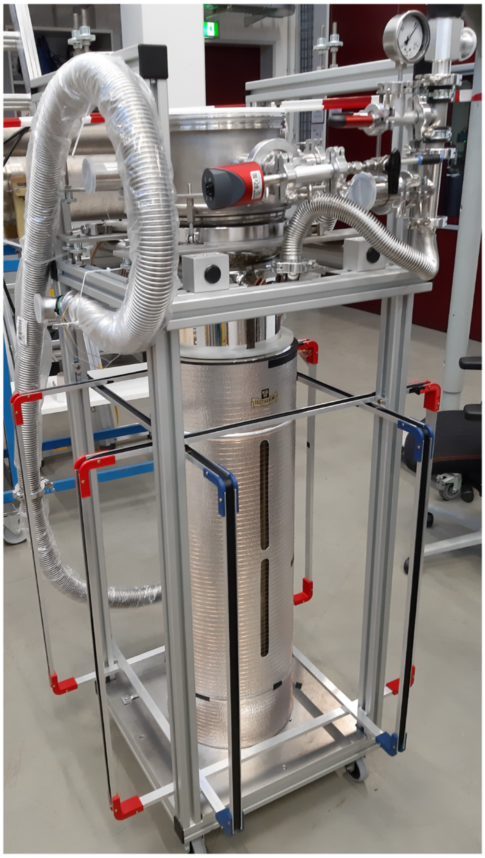

FIG. 1. Picture of a cryostat with coils for active magnetic field compensation. The two rectangular Helmholtz-coils (red and blue corners) create magnetic field in horizontal directions. The solenoid wound around the aluminum housing creates a field in the vertical direction.

The dimensions of the solenoid are predetermined by the dimensions of the aluminum housing. It has a radius of $r = 14.5$ cm and a length of $l = 88$ cm. The distance between windings was chosen to be 1 cm, resulting in 88 windings.

The rectangular design of the HHC slightly alters the Helmholtz condition[9] to

$$\frac{h}{2} = 0.5445 \times a, \tag{1}$$

where h is the distance between the two coils and $2a$ is the side length of the coils. One pair is mounted to the inside of the aluminum frame of the cryostat (red coil shown in Fig. 1). This fixes the distance h and, therefore, side lengths of one of the Helmholtz-coil pairs. The side lengths of the other coil are chosen such that it just fits inside the first one.

The coils are built with aluminum U-profiles with a width of 2 cm, height of 1 cm, and wall thickness of 0.2 cm. The profiles are connected via 3D-printed connectors (red and blue corners shown in Fig. 1). The coil dimensions are presented in Table I. Both pairs have 75 windings on each coil.

In order to estimate the field flatness of the coils, COMSOL[10] simulations were performed. From these simulations, several parameters were extracted: the coil constant $\gamma = B/I$, where B is the maximum flux density generated by a current I, the field flatness ϕ, and maximal percentage stray field σ.

ϕ is given by the ratio of minimum and maximum magnetic flux densities created by the coil in the sample volume. The parameter σ is obtained by dividing the maximum field perpendicular to the design direction[11] by the maximum field in design direction within the sample volume. The sample is a sheet of dimensions $100 \times 60 \times 3\ \text{mm}^3$ and centered on the coils. The sample face is aligned with the blue HHC. In case of the solenoid, the sample center is 5 cm above the center of the coil. Table I presents the parameters of all three coils.

An iterative magnetic field compensation scheme was implemented employing three single-axis fluxgate magnetometers, which are aligned to measure the magnetic field in 3D close to the sample (the setup is described in more detail in Sec. III). They serve as reference for the compensation. With the measured coil constant presented in Table I, the currents for all three coils are calculated that should compensate the field measured by the fluxgates and applied to the coils. Since the coils are not aligned perfectly (misalignment $\approx 1^\circ - 2^\circ$), the compensation does not work perfectly in the first step. Therefore, the compensation is done iteratively: In the next step, the residual magnetic field is remeasured, and the coil currents are readjusted to reduce the field further. This procedure is repeated until a residual field of no more than 25 nT is achieved. This scheme is completely automated.

The same scheme can, of course, also be used to set an arbitrary field.

TABLE I. Technical data for the coils integrated into the small bath cryostat. Field flatness and the field in a non-dominant direction are calculated in the sample volume. The maximum flux density stated here is reached with a power supply limited at 70 V and 1.5 A.

	Solenoid	HHC large	HHC small
Side-length $2a$ (cm)	29	73.4	71.4
Coil distance h (cm)	88	40	38.9
Number of windings	88	75	75
Coil constant γ (sim.) (μTA^{-1})	117.9	164.2	169.0
Coil constant γ (meas.) (μTA^{-1})	117.6	165.4	169.9
Max. achievable flux density (μT)	180	190	190
Field flatness ϕ	0.992	>0.999	>0.999
Max. stray fields σ (%)	0.3	<0.1	<0.1

III. SETUP TO MEASURE TRAPPED FLUX IN SAMPLES

In this section, the core setup is described. First, the sample geometry is introduced together with the considerations leading to this geometry. Then, the mounting and temperature control are described. Last, the sensors for measuring temperature and magnetic field are introduced.

A. The sample

To keep the geometry simple, the sample shape is chosen to be a flat, rectangular sheet. The rectangular shape was chosen so that when the sample is cooled down, the phase front, which marks the transition between a normal and superconducting phase, is a straight line. This reduces the impact of geometry compared to a round sample. The thickness of the sheet is chosen to be 3 mm, which is the typical wall thickness of cavities. The other two dimensions should be large enough to be able to place several magnetic field sensors above the sample and also not be dominated by effects on the sample's edges.

The $(100 \times 60 \times 3)\ \text{mm}^3$ provides room for an array of 3×5 magnetic field sensors distributed over the sample surface. To investigate whether the measurements are influenced by edge effects, COMSOL simulations were carried out. In these simulations, a remanent flux density of 100 μT is set in the sample and the resulting magnetic field at the sensor positions is simulated. To investigate the edge effects, the remanent flux density in a rim with a width of 1 mm around the sample is changed. In one simulation, it is set to 0 μT, in a second to 300 μT. The difference of (simulated) flux density at the sensor positions between the two cases is, in the worst case, 0.2 μT. This is not significant compared to other error sources in the magnetic field measurements (inhomogeneities in the external magnetic field and inconsistencies in cooldown dynamics). The sensor response, therefore, appears insensitive to the details at the sample edge.

B. Temperature control

To control the temperature gradient across the sample during cooldown, the temperatures at the ends of the sample must be independently adjustable. Furthermore, the experiment must allow heating the sample above its transition temperature in order to release the trapped flux and perform multiple cooldowns under reproducible starting conditions. Since niobium has a critical temperature of 9.2 K, the setup is not submerged in liquid helium but is suspended in the vapor above. A heater in the helium bath is used to evaporate helium and create a constant flow of cold gas to cool down the sample below T_c. This is schematically shown in Fig. 2. In the real experiment, the setup is mounted to titanium threaded rods hanging from the top lid of the cryostat.

To control the temperature gradient across the sample, electric heaters are used. As they create a magnetic field, the heaters are not directly mounted to the sample but to copper blocks, which provide sufficient distance for the heater field to be negligible. These copper blocks are, in turn, clamped to the sample (see Fig. 2). To clamp the copper blocks, a slit with a width of 3.1 mm and depth of 20 mm is milled in their ends. The sample is slid in the top 2 mm of this slit,

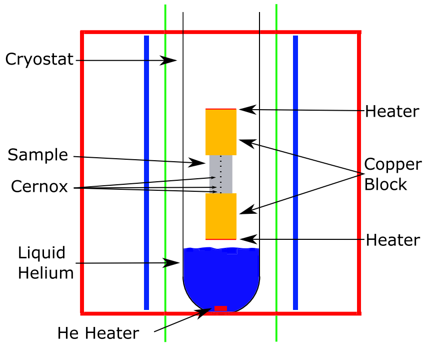

FIG. 2. Schematic of the setup in the cryostat. The sample is clamped in two copper blocks with heaters attached to them. An additional heater in the helium bath is used to create a constant flow of cold helium gas. To measure the temperature gradient, eight Cernox sensors are glued directly to the sample. Two Helmholtz coils (red and blue) and a solenoid (green) arranged perpendicularly to each other around the cryostat can generate a magnetic field with arbitrary orientation. The details of the sample and copper blocks are shown in Fig. 3, while the sensor setup with the AMRs and fluxgate sensor are shown in Fig. 4.

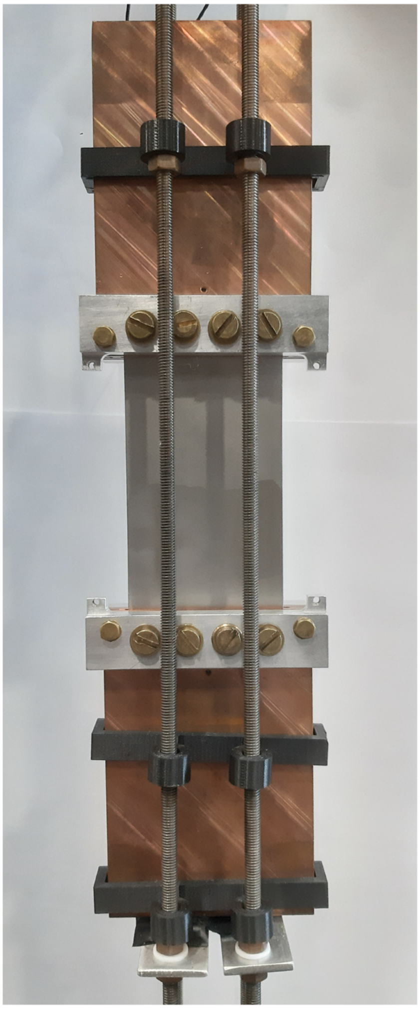

FIG. 3. Picture of the partially assembled setup. The sample is clamped in two copper blocks. The aluminum blocks under the bolts distribute the force more evenly. The whole setup is suspended in the cryostat using titanium threaded rods hanging from the top lid.

which is then compressed by 6 bolts. In addition, 10 mm thick aluminum blocks are used as "washers" to spread the force more evenly. By clamping the sample like this, no holes need to be drilled in the sample, which would complicate the expulsion mechanism and have an unpredictable influence on flux trapping. A picture of the partially assembled setup is shown in Fig. 3.

To control the temperature and temperature gradient, both heaters are independently controlled by PID controllers implemented in LabView.[12] As a reference temperature, the two Cernox sensors on the sample closest to the sample edge are used (see Sec. III C 1). The individual heater powers are adjusted in a range of 0–25 W. The PID controllers adjust the power every 100 ms, which enables rapid changes in temperature. The power of the heater submerged in the liquid is typically set in a range of 5–10 W. With this configuration, a temperature gradient in the range of (0–0.3) K cm^{-1} can be achieved. This is comparable with the cavity measurements performed at Fermilab[3] and other flux trapping experiments.[13]

C. Sensors

1. Temperature sensors

To measure the temperature gradient along the sample, eight Cernox sensors type CX-SD 10-50 are used.[14] They are glued along a vertical line in the middle of the sample using silver conductive paint. In addition, three Cernox sensors type CU are used. One is mounted on each of the copper blocks, and the third measures the gas temperature next to the sample.

The temperatures are recorded with a temperature monitor 218 by Lakeshore.[15] This device has a resolution of 100 mΩ, which corresponds to a temperature resolution of roughly 0.5 mK at 9 K. The drawback of the temperature monitor is its slow read out frequency of only 2 Hz. Since this is not sufficient to monitor fast cooldowns, alternatively a SPARTAN analog-digital converter (ADC) by imc[16] can be used to measure the voltage drop across the sensors and, hence the temperature. In its smallest measurement range of ±50 mV, its 16-bit resolution results in a voltage resolution of 3.05 μV. With a driving current of 10 μA from the Lakeshore device, this results in a resolution with resistance of 300 mΩ, or roughly 1.5 mK temperature resolution. Although it has a lower voltage resolution, the measurement rate can be increased up to 500 Hz. However, in experiments, the rate is kept below 100 Hz to decrease noise.

To measure the temperature with the imc device, the Lakeshore device is used as a constant current source, but the leads for the voltage measurement are fed into a relay box. In this box, the connection can be switched between the Lakeshore and imc device. The devices cannot be connected at the same time as their apparent impedance mismatch falsifies the measurement. As the value recorded by the imc device differs from the one recorded by the Lakeshore device, the calibration curves provided by the manufacturer cannot be used but a new calibration curve must be taken for the imc device. It is obtained by switching between Lakeshore and imc devices to record the temperature and corresponding imc-voltage while the sample slowly warms up after a filling procedure.

2. Magnetic field sensors

The magnetic field is measured using two different sensor types: fluxgate sensors and anisotropic magnetoresistive (AMR) sensors.[17] The fluxgate sensors are used as reference for the AMR sensors and active field compensation. The AMR sensors are mounted as close as possible to the sample and are used to measure trapped flux.

Three single-axis fluxgate probes Mag-F are used in combination with the Mag-01H readout by Bartington[18] to measure the magnetic field in 3D. They are mounted with a 3D-printed fixture to the threaded rods hanging from the top lid. This aligns the sensors orthogonally to each other and in line with the coils. Since the inhomogeneities in the external field cannot be compensated by the coils, it is important that the sensors are as close to the AMR sensors and the sample as possible. Figure 4 shows a picture of the fluxgate sensors in relation to the sample.

To measure trapped flux, AMR sensors are used because they are much smaller (~ 10 mm^2 wafer instead of 20 mm long cylinder) and cheaper (~1€ instead of ~1000€) compared to fluxgate sensors. They are soldered to a custom printed circuit board (PCB), which combines three sensors to one sensor group to measure the full 3-D field vector. To measure the magnetic field perpendicular to the sample surface, one of the sensors must be rotated to be perpendicular to the main PCB. This is done using small adapter PCBs, which are soldered perpendicular to the main board in routed slits in the latter. The other two sensors are soldered directly onto the board on opposite sides and rotated by 90° with respect to each other. The groups are arranged in an array of 3 × 5, which are 13 mm apart horizontally and 16 mm apart vertically allowing for a mapping of the field vector. The sensor group in the middle is centered on the sample. The sensors closest to the sample surface are the sensors measuring in the horizontal direction, parallel to the surface; they are 2.5 mm away from the surface. The sensors measuring the field perpendicular to the surface are 3.8 mm from the surface and the sensors measuring the vertical direction are 5.1 mm. The vertical distance between the sensor measuring perpendicular to the surface and the other two is 5 mm.

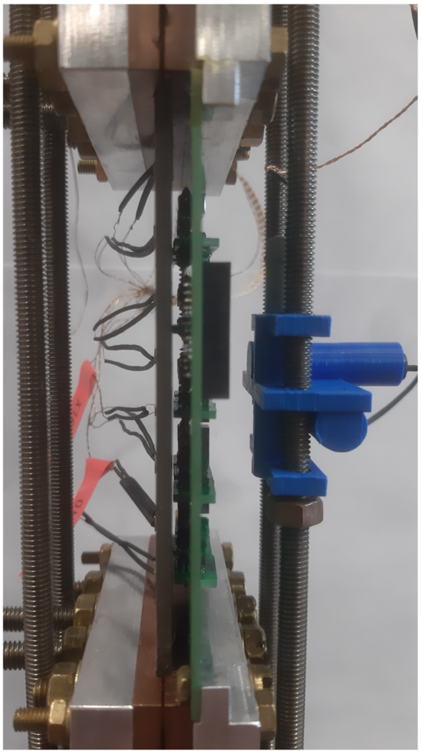

FIG. 4. Side view of the setup with mounted fluxgates in 3D-printed fixture (blue). The AMR sensors are mounted between fluxgate sensors and the sample on the green PCB. Cernox sensors are glued to the left side of the sample.

To calibrate AMR sensors, they have a built-in coil, which can be used to flip the magnetization of the active elements of the AMR sensors 180°. This way, an offset calibration can be performed. However, at cryogenic temperatures, this flip does not work consistently so they cannot be operated in the intended way. They are, therefore, calibrated with the help of the fluxgate sensors. Details on the AMR sensors and their use in the cryogenic environment can also be found in previous studies.[19,20]

During soldering, the sensors are not perfectly orthogonally arranged. In addition, the mounted PCB is not perfectly aligned with the coordinate system of the HHC and fluxgate sensors. It is necessary to know the misalignment of all sensors with respect to the coordinate system of the fluxgate sensors, which is used as reference. This information can be gained during calibration with the three HHC by expressing the output voltage of a whole sensor group as a system of linear equations. Using these equations, the sensitivity of each sensor in all directions can be obtained. With these sensitivities, the misalignment of the sensors is considered in the measurement.

The output voltages of the AMR sensors of one group in dependence of the magnetic field components can be expressed as

$$\begin{aligned} V_x &= \alpha_x B_x + \beta_x B_y + \gamma_x B_z + \delta_x, \\ V_y &= \alpha_y B_x + \beta_y B_y + \gamma_y B_z + \delta_y, \\ V_z &= \alpha_z B_x + \beta_z B_y + \gamma_z B_z + \delta_z, \end{aligned} \tag{2}$$

where V_i is the output voltage of the sensor with dominant measurement direction in the i direction and B_i are the flux density components. $\alpha_i, \beta_i, \gamma_i, \delta_i$ are fit parameters. δ_i is the offset voltage of a sensor, and $\alpha_i, \beta_i, \gamma_i$ are equal to the sensitivities of every sensor in each direction. Equation (2) can also be expressed as

$$\vec{V} = \mathbf{S}\vec{B} + \vec{V_0}. \tag{3}$$

Here, $\mathbf{S}$ is the sensitivity matrix and $\vec{V_0}$ are the offset voltages. If the sensors were aligned perfectly, $\mathbf{S}$ would have entries only on the diagonal.

To determine the sensitivities and offset values, 15 different magnetic fields are applied with the coils. After each field is set, the output voltages of the sensors V_i and the magnetic flux density measured by the fluxgates $\vec{B}$ are stored. Then a 4-dimensional linear fit is performed for each sensor according to the corresponding equation in Eq. (2) to determine the fit parameters. To measure magnetic flux density with one sensor group, the output voltages $\vec{V}$ are measured. Since **S** and $\vec{V_0}$ are known from the fit, the system of linear equations in Eq. (3) can be solved numerically for $\vec{B}$. The calibration is redone for each cooldown from room temperature.

The offset error of this calibration is up to 0.2 μT, and the relative error is less than 1%. The drawback of this calibration method is that all sensors are calibrated to the three fluxgate sensors, which measure magnetic field at only one position. Any inhomogeneities in the field are, thus, unaccounted for and cannot be measured with the AMR sensors. The absolute values are only reliable within the margins of the inhomogeneities of the ambient magnetic field. To estimate these inhomogeneities, the cryostat is moved 10 cm back and forth in every horizontal direction, and the lid is lifted up 10 cm while fluxgate sensors record the magnetic flux density. With these measured changes in flux density, the field variation within the sample volume was estimated. This, of course, depends on the environment in which the cryostat is set up. At the current location, the worst case estimation yields inhomogeneities of 2.3 μT. The systematic measurement error of the AMR sensors is, therefore, considered to be 2 μT.

D. Measurement procedure

For the first cooldown, liquid helium is filled in the cryostat until the liquid level is just below the lower copper block. Due to the evaporating helium, the sample is cooled below T_c during this filling procedure for the first time. After the filling is completed, a constant power (typically 5–10 W) is applied to the heater submerged in the liquid to create a continuous flow of cold helium gas. The power is adjusted according to the desired cooldown: For fast cooldowns, a higher gas flow is required so the heater power is set to a high value (e.g., about 10 W). For slow cooldowns, this is not necessary so the heater power can be decreased to conserve helium (about 5 W). The detailed control of the cooldown rate, however, is performed by regulating the heaters on the copper blocks (see below). Then, the heaters on the copper blocks are used to heat the sample above T_c. Once the sample is normal, conducting the active field compensation can be used to compensate the external magnetic field to zero. When the field compensation is completed, the coil currents are stored. Then, a flux density is set for the cooldown (e.g., 100 μT perpendicular to the sample surface). To achieve a temperature gradient across the sample, the setpoint temperatures of both heaters are set at different values above T_c. For example, to achieve a temperature gradient of 0.06 K cm^{-1}, the temperature of the bottom edge of the sample is set at 9.5 K and the top edge at 10.1 K. Since the sample is 10 cm long, this yields the desired gradient. After the temperatures have settled, the set temperatures of both heaters are lowered simultaneously. This ensures a constant temperature gradient during cooldown while the sample becomes superconducting from bottom to top. The cooldown rate is controlled by adjusting the rate at which the set temperatures are lowered. Figure 5 shows an exemplary temperature profile during cooldown. Since the temperature differences between the four depicted Cernox sensors which are glued in a vertical line on the sample stay constant during cooldown, the temperature gradient is constant as well.

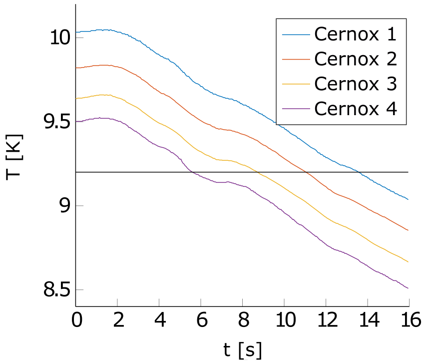

FIG. 5. Exemplary temperature profile during cooldown recorded with four Cernox sensors. The sensors are label 1–4, with 1 being at the top and 4 at the bottom of the sample. Since the four lines stay equidistant, a constant temperature gradient is established during the cooldown. In addition, the critical temperature of 9.2 Kis is indicated in black.

When the sample is fully superconducting, the previously stored coil currents for the zero-field are set again in the coils. This way, the external magnetic field is compensated and only the flux trapped inside the sample is measured by the AMR sensors. The data obtained at this stage are the values of trapped flux that are presented further in Sec. IV. After the magnetic field is recorded, the set temperatures of the heaters are again increased above T_c and the next cooldown with different cooldown parameters is performed.

IV. MEASUREMENT RESULTS

In this section, exemplary measurement results are provided to illustrate the data that can be obtained with the apparatus. The effects of temperature gradient, cooldown rate, and external magnetic field on trapped flux were studied. Three different sample types were studied: large-grain bulk niobium, fine-grain bulk niobium, and a sample consisting of a copper substrate with a niobium film sputtered onto it.

The large-grain (RRR = 300) sample consists of only two grains with a grain boundary running horizontally through the sample. The sample is cut out of a 3 mm sheet with a water jet and was left completely untreated. This means that approximately the first 100 μm below the surface are comprised of a damaged layer. In this layer, the crystal structure is compromised, which might have an influence on flux trapping behavior. However, since the first test is intended as a baseline test, this layer is not removed. In the future tests, a buffered chemical polish (BCP) will be performed to remove this layer.

The fine-grain sample is also cut with a water jet from a RRR = 300 niobium sheet that was intended for cavity fabrication. The grain size is in the order of 100 μm. As this sample is also completely untreated, a damage layer is also present.

The coated sample was prepared by the group "Oberflächentechnik" from Universität Siegen. It consists of a copper substrate that is mechanically polished up to 4000 grit and subsequently sputtered with a 4 μm thick niobium layer. For best coating results, the copper should be chemically polished before coating.[21] However, due to time restrictions, this step was skipped. The quality of the coating can, therefore, be improved in future tests.

A. Temperature gradient

Many studies have investigated the effect of temperature gradient on trapped flux.[3,22,23] The studies show that a larger temperature gradient during cooldown leads to less trapped flux. This dependency can now be investigated in more detail with this new setup because many more temperature cycles are possible.

During the cooldown cycles, the temperature gradient was varied but all other parameters were kept constant. The applied magnetic flux density was set at 100 μT perpendicular to the large sample surface, and the cooldown rate was set at 0.07 K s^{-1}. The temperature gradient can be varied in a range of $\approx(0.01 - 0.3)$ K cm^{-1}. The maximum gradient is smaller by about a factor of two compared to what can be achieved for cavities: $\lesssim 0.4$ K cm^{-1} in Ref. 24 or up to 0.8 K cm^{-1} in Ref. 22.

Figure 6 shows trapped magnetic flux $|B_{TF}|$ measured by the central sensor group vs the local temperature gradient during cooldown. To calculate the local temperature gradient, the temperature difference between one Cernox sensor and the sensor above it is determined when the sensor passes the transition temperature of 9.2 K. The temperature difference is then divided by the distance between the two sensors. To estimate the error of the temperature gradient, the local gradient is calculated for every sensor. From these values, the mean temperature gradient and error of a single measurement are calculated.

At temperature gradients close to zero, nearly all flux is trapped in all samples. However, with increasing temperature gradient, the three samples show different behaviors. In case of the large-grain sample, a sharp decrease in trapped flux is measured up to $\approx$0.1 Km^{-1}. At this point, full expulsion (within the measurement error) is achieved. In case of the fine-grain sample, the decrease is less steep and full expulsion is not achieved. In case of the coated sample, no dependency of trapped flux on temperature gradient is evident. A limiting feature of the measurements with this sample is that the temperature sensors were glued to the copper substrate and not the niobium film. The actual temperature profile of the film is, therefore, not known. The temporal correlation of signals in the magnetic field sensors to the temperature sensors suggest that the temperature profile of the film is at least close to the measured one. Furthermore, the heat transport happens nearly exclusively via the copper substrate, and the film will take the temperature of the underlying copper as long as there is some adhesion of the film to the substrate. However, inhomogeneities and formation of superconducting islands cannot be excluded. In future experiments, some of the sensors should be glued to the film. In addition, further studies of the grain structure are necessary to gain more insight into why it expels flux so poorly. The poor expulsion of the film indicates that a 4 μm thick layer can have a strong influence on the flux trapping behavior of a material.

B. External magnetic field strength

The effect of flux density magnitude on trapped flux is measured by keeping the temperature gradient and cooldown rate constant within one measurement series. The orientation of the external field is also kept constant, pointing perpendicular to the large sample surface. The magnetic flux density is then altered from −180 to +200 μT within a series. Once a complete series is recorded, another series with a different temperature gradient is recorded. Figure 7 shows three measurement series obtained with the large-grain sample.

Figure 7 shows that for $\nabla T = 0$ K cm^{-1}, trapped flux increases linearly with increasing external flux density. However, for temperature gradients larger 0 K cm^{-1}, flux is only trapped once the external flux density magnitude exceeds a threshold level. The magnitude of this threshold depends on the temperature gradient. Above the threshold field, the increase is again linear. However, the slope decreases with increasing temperature gradient. To our knowledge, the occurrence of this threshold field has not been observed before and further investigations are necessary to understand its origin. One should note that the threshold field cannot directly be translated to cavities as the complex geometry affects flux trapping behavior and the material goes through many different steps

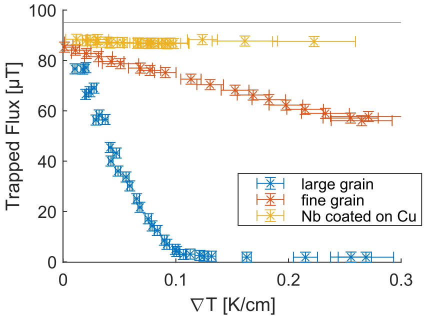

FIG. 6. Trapped flux measured by the central sensor group vs local temperature gradient. Measured data of all three samples are depicted. While trapped flux decreases with higher temperature gradient for the large and fine-grain sample, no dependency is evident for the coated sample. A difference between large and fine-grain is also clearly visible. With the large-grain material, full flux expulsion is possible for temperature gradients above 0.1 K cm^{-1}. The gray line indicates the expected flux density measured, if 100% of the flux is trapped. This value is obtained with COMSOL simulations.

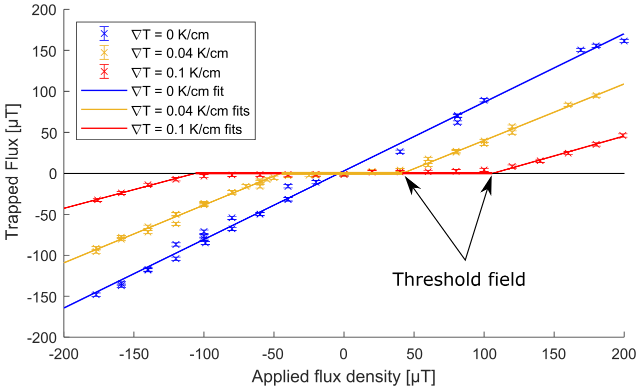

FIG. 7. Trapped flux measured by the central sensor group vs external flux density. The field orientation is kept constant, perpendicular to the sample surface. The different colors depict different series recorded at different temperature gradients. Flux is only trapped once a temperature-gradient threshold field is exceeded. Data points above the threshold field are fitted using a linear regression.

during fabrication that are not necessarily reflected by our sample preparation.

In case of the fine-grain sample, no threshold field was observed. However, similar to the large-grain sample, the slope of the linear fits decreases with increasing temperature gradient.

Since the coated sample always traps all flux, no dependence on external flux density is evident.

C. Cooldown rate

To measure the effect of cooldown rate on trapped flux, both the ambient magnetic flux density (100 μT perpendicular to the sample surface) and the temperature gradient are kept constant within one series. The cooldown rate is then altered for repeated cooldowns. It is varied in a range of $\approx (0–2)\ \mathrm{K\ s^{-1}}$. For cavity measurements, the range is typically $\approx (0–0.2)\ \mathrm{K\ s^{-1}}$ (see Ref. 22). Figure 8 shows the measurement data for trapped flux vs transition time measurements obtained with the large-grain sample. Here, transition time (t_T) denotes the time it takes for the sample to become fully superconducting once the bottom reaches T_c. As the sample is 10 cm long, t_T is related to the cooldown rate $\mathrm{d}T/\mathrm{d}t$ and the temperature gradient ∇T via $t_\mathrm{T} = \frac{\nabla T \times 10\ \mathrm{cm}}{\mathrm{d}T/\mathrm{d}t}$.

Figure 8 shows that at very short transition times (or high cooldown rates), trapped flux is nearly independent of the temperature gradient and ≈74 % of the applied field are trapped for the highest temperature gradient of $0.1\ \mathrm{K\ cm^{-1}}$. Trapped flux then sharply decreases up to a transition time of ≈1 s, which is followed by a less steep decrease of up to ≈6 – 7 s. For even longer transition times, trapped flux seems to be independent of transition time.

Data obtained with the fine-grain sample show the same time constants. However, of course, the trapped flux magnitudes are higher. Similar to before, no dependence is evident for the coated sample.

The increase in trapped flux toward shorter transition times is an unexpected result, since typically the flux expulsion efficiency is considered to be independent of cooldown rate.[24,25] These measurements, however, show that is not the case for very high cooldown rates. As these high rates are not obtained with usual filling procedures in cavity tests, it is not surprising that this effect has not been observed before. This phenomenon is investigated in more detail in Ref. 7.

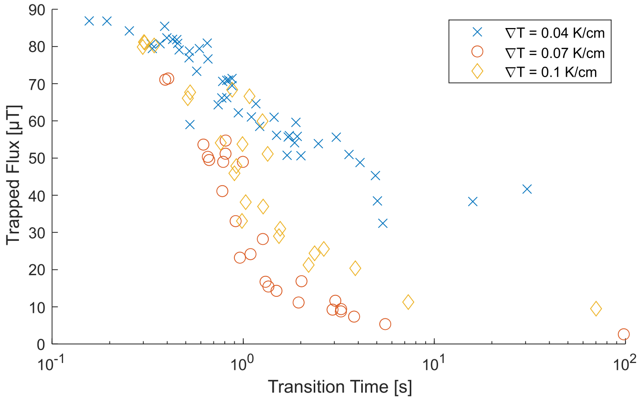

FIG. 8. Trapped flux measured by the central sensor group vs transition time for the large-grain sample. Transition time denotes the time it takes for the sample to become fully superconducting once it starts at the bottom. Each color denotes a series recorded at nominally the same temperature gradient. The data show a sharp increase in trapped flux for transition times shorter than ≈1 s. The logarithmic time axis should be noted.

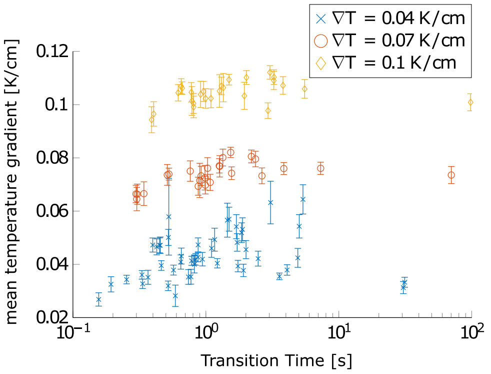

FIG. 9. Corresponding temperature gradients to the cooldowns shown in Fig. 8. The data points are obtained from the same cooldowns, only that now the temperature gradient instead of the trapped flux is plotted.

In Fig. 8, we observe a fairly large scatter in the data, which, in part, is due to the fact that especially fast cooldowns with small temperature gradients are difficult to control with respect to constant temperature gradient and cooldown rate during the cooldown. The inconsistencies in cooldown dynamics arise because fast cooldowns are harder to control accurately since the heater power must be changed in large steps to achieve these cooldown rates and there is less time for corrections. This is shown in Fig. 9 where the temperature gradients of the same cooldowns as in Fig. 8 are shown. A large scatter in temperature gradient is evident, especially for $\nabla T = 0.04\ \mathrm{K\ cm^{-1}}$, which translates to a large scatter of trapped flux shown in Fig. 8. This error could be reduced by excluding points with a large deviation from the desired temperature gradient. However, for the purpose of presenting the capabilities and limitations of the setup, they are kept in these plots. At small temperature gradients and high cooldown rates, the phase front might also not move continuously through the sample, but spontaneous nucleation of superconducting regions might occur. This would also increase the scatter in the data. As is shown in Fig. 8, the error is larger than the 2 μT estimated above.

V. CONCLUSION AND OUTLOOK

The results presented in Sec. IV demonstrate the capabilities and advantages of this setup: The independent control of parameters such as the temperature gradient, cooldown rate, and ambient magnetic field, as well the fast thermal cycles, make it possible to investigate the effects of these parameters on trapped flux in great detail.

The active magnetic field compensation proved to be a good alternative to magnetic shielding as it is much cheaper. Importantly it allows us to the application of an arbitrarily orientated external magnetic field with an accuracy of 25 nT at the position of the reference sensors and a homogeneity across the sample of ~2 μT. Future measurement campaigns are planned to illuminate the effect of orientation of the external field with respect to the sample. In the future, homogeneity can be improved by adding passive shielding around the cryostat and the Helmholtz coils to reduce the ambient magnetic field or at least make it more homogeneous. This could enable measurements in the sub μT range, which is where SRF cavities are typically operated currently.

The temperature control with two independent heaters worked well, and a parameter space comparable with other (cavity) experiments can be mapped out systematically. However, inconsistencies in the cooldown dynamics, such as non-homogeneous temperature gradient and cooldown rate during cooldown, are also the largest source of error of this setup, as can be seen in Sec. IV C. To reduce the impact of the helium atmosphere on the cooldown, the sample could be encapsulated in a vacuum chamber in the future.

The unexpected results of the observed threshold field in Sec. IV B and the impact of cooldown rate in Sec. IV C show the importance of sample measurements in order to get a better understanding of flux trapping. The different behaviors of the samples in Sec. IV A also show how differently materials react to changes under cooldown conditions. Considering the improved statistics that can be obtained with this setup, it can give important insights into the flux trapping mechanism, which can ultimately be used to increase the performance of SRF cavities.

ACKNOWLEDGMENTS

This work was partially funded by the German BMBF Verbundprojekt Grant No. 05K2022 - NOVALIS: Innovative Beschleunigertechnologien für effiziente Strahlungsquellen.

AUTHOR DECLARATIONS

Conflict of Interest

The authors have no conflicts to disclose.

Author Contributions

F. Kramer: Conceptualization (equal); Data curation (lead); Formal analysis (lead); Methodology (equal); Software (lead); Visualization (lead); Writing – original draft (lead). **S. Keckert**: Methodology (equal); Software (supporting); Writing – review & editing (equal). **O. Kugeler**: Conceptualization (equal); Funding acquisition (equal); Methodology (equal); Supervision (equal); Writing – review & editing (equal). **J. Knobloch**: Conceptualization (equal); Funding acquisition (equal); Methodology (equal); Supervision (equal); Writing – review & editing (equal).

DATA AVAILABILITY

The data that support the findings of this study are available from the corresponding author upon reasonable request.

REFERENCES

[1] T. Matsushita, *Flux Pinning in Superconductors*, 3rd ed., *Springer Series in Solid-State Sciences* (Springer, Cham, 2022), Vol. 198.

[2] A. Gurevich and G. Ciovati, "Effect of vortex hotspots on the radio-frequency surface resistance of superconductors," Phys. Rev. B **87**, 054502 (2013).

[3] S. Posen, G. Wu, A. Grassellino, E. Harms, O. S. Melnychuk, D. A. Sergatskov, N. Solyak, A. Romanenko, A. Palczewski, D. Gonnella, and T. Peterson, "Role of magnetic flux expulsion to reach $Q_0 > 3 \times 10^{10}$ in superconducting rf cryomodules," Phys. Rev. Accel. Beams **22**, 032001 (2019).

[4] T. Okada, E. Kako, M. Masuzawa, H. Sakai, R. Ueki, K. Umemori, and T. Tajima, "Observation of quenching-induced magnetic flux trapping using a magnetic field and temperature mapping system," Phys. Rev. Accel. Beams **25**, 082002 (2022).

[5] S. Posen, M. Checchin, A. C. Crawford, A. Grassellino, M. Martinello, O. S. Melnychuk, A. Romanenko, D. A. Sergatskov, and Y. Trenikhina, "Efficient expulsion of magnetic flux in superconducting radiofrequency cavities for high Q applications," J. Appl. Phys. **119**, 213903 (2016).

[6] F. Kramer, O. Kugeler, J.-M. Köszegi, and J. Knobloch, "Impact of geometry on flux trapping and the related surface resistance in a superconducting cavity," Phys. Rev. Accel. Beams **23**, 123101 (2020).

[7] F. Kramer, Impact of cooldown conditions on trapped flux in superconducting niobium, Ph.D. thesis, Universität Siegen, 2024.

[8] F. Kramer, S. Keckert, O. Kugeler, T. Kubo, and J. Knobloch, "Study of the dynamics of flux trapping in different SRF materials," in *Proceedings of the 21st International Conference on Radio-Frequency Superconductivity (SRF'23)* (JACoW, Grand Rapids, MI, 2023), Vol. 21, pp. 380–387.

[9] A. R. Alvarez, E. Franco-Mejía, and C. R. Pinedo-Jaramillo, "Study and analysis of magnetic field homogeneity of square and circular Helmholtz coil pairs: A Taylor series approximation," in Proc. 2012 Andean Region International Conference, 2012.

[10] COMSOL AB, Comsol multiphysics v (2021), Vol. 60.

[11] The design direction is defined to be perpendicular to the coil faces.

[12] NI, Labview version: 2016 (2016).

[13] D. Turner, A. G. Terricabras, I. G. Díaz-Palacio, W. Hillert, T. Koettig, A. Macpherson, G. Rosaz, N. Stapley, and M. Wenskat, "Flux expulsion lens: Concept and measurements," in *Proc. 21th Int. Conf. RF Supercond. (SRF'23)* (JACoW, Grand Rapids, USA, 2023), Vol. 21, pp. 56–61.

[14] Lake Shore Cryotronics, Cernox® (2023).

[15] Lake Shore Cryotronics, Inc., Model 218 (2017).

[16] Imc Test & Measurement GmbH, Imc spartan (2023).

[17] Sensitec GmbH, AFF755B MagnetoResistive field sensor (2018).

[18] Bartington Instruments Ltd, Mag-01H (2023).

[19] B. Schmitz, J. Köszegi, K. Alomari, O. Kugeler, and J. Knobloch, "Magnetometric mapping of superconducting RF cavities," Rev. Sci. Instrum. **89**, 054706 (2018).

[20] F. Kramer, *Mapping Trapped Flux and the Related Surface Resistance in Superconducting Cavities* (Universität Siegen, 2019).

[21] O. Malyshev, C. Antoine, O. Azzolini, G. Burt, E. Chyhyrynets, P. Goudket, G. Keppel, O. Kugeler, S. Leith, A. Medvids, P. Onufrijevs, C. Pira, R. Ries, D. Seal, E. Seiler, A. Sezgin, B. Sian, F. Stivanello, A. Sublet, D. Tikhonov, D. Turner, R. Valizadeh, G. Vandoni, L. V. Cid, W. V. Delsolaro, P. V. García, and M. Vogel, "Main highlights of ARIES WP15 collaboration," in *Proc. 20th International Conference on RF Superconductivity (SRF'21)* (JACoW, Geneva, Switzerland, 2022), pp. 571–575.

[22] S. Huang, T. Kubo, and R. L. Geng, "Dependence of trapped-flux-induced surface resistance of a large-grain nb superconducting radio-frequency cavity on spatial temperature gradient during cooldown through tc," Phys. Rev. Accel. Beams **19**, 082001 (2016).

[23] A. Romanenko, A. Grassellino, A. C. Crawford, D. A. Sergatskov, and O. Melnychuk, "Ultra-high quality factors in superconducting niobium cavities in ambient magnetic fields up to 190 mG: Applied physics letters," Appl. Phys. Lett. **105**(23), 234103 (2014).

[24] A. Romanenko, A. Grassellino, O. Melnychuk, and D. A. Sergatskov, "Dependence of the residual surface resistance of superconducting radio frequency cavities on the cooling dynamics around T_c," J. Appl. Phys. **115**, 184903 (2014).

[25] M. Wenskat and J. Schaffran, "Analysis of the cool down related cavity performance of the european X-ray free electron laser vertical acceptance tests," AIP Adv. **7**, 115110 (2017).